J. Fluid Mech. (2012), *vol.* 709, *pp.* 581–592.
doi:10.1017/jfm.2012.350

On the acoustic levitation stability behaviour of spherical and ellipsoidal particles

D. Foresti, M. Nabavi and D. Poulikakos†

Department of Mechanical and Process Engineering, Institute of Energy Technology, Laboratory of Thermodynamics in Emerging Technologies, ETH Zurich, CH-8092, Zurich, Switzerland

(Received 3 April 2012; revised 4 June 2012; accepted 3 July 2012;
first published online 31 August 2012)

We present here an in-depth analysis of particle levitation stability and the role of the radial and axial forces exerted on fixed spherical and ellipsoidal particles levitated in an axisymmetric acoustic levitator, over a wide range of particle sizes and surrounding medium viscosities. We show that the stability behaviour of a levitated particle in an axisymmetric levitator is unequivocally connected to the radial forces: the loss of levitation stability is always due to the change of the radial force sign from positive to negative. It is found that the axial force exerted on a sphere of radius R_s increases with increasing viscosity for $R_s/\lambda < 0.0125$ (λ is the acoustic wavelength), with the viscous contribution of this force scaling with the inverse of the sphere radius. The axial force decreases with increasing viscosity for spheres with $R_s/\lambda > 0.0125$. The radial force, on the other hand, decreases monotonically with increasing viscosity. The radial and axial forces exerted on an ellipsoidal particle are larger than those exerted on a volume-equivalent sphere, up to the point where the ellipsoid starts to act as an obstacle to the formation of the standing wave in the levitator chamber.

Key words: drops, wave scattering, wave–structure interactions

1. Introduction

In acoustic levitation, the acoustic radiation pressure is used to overcome gravitational force. Owing to its material independency, acoustic levitation has found a wide spectrum of applications in contactless processing and analysis of liquid samples (Trinh, Thiessen & Holt 1998; Yarin, Pfaffenlehner & Tropea 1998). The contactless manipulation and transportation of particles and droplets is one of the most interesting challenges in the acoustic levitation field (Koyama & Nakamura 2010; Foresti *et al.* 2011; Foresti, Nabavi & Poulikakos 2012) with applications ranging from the handling of living cells in lab-on-a-chip devices (Bruus *et al.* 2011) to millimetre-size sample manipulations in air (Bjelobrk *et al.* 2010).

The most common acoustic levitator studied in the literature is the axisymmetric levitator. In such a levitator, the sample is trapped at a pressure node at a stable position. Studies of axisymmetric levitators have been conducted by means of analytical solutions and numerical methods assuming an ideal fluid (Barmatz & Collas 1985; Xie & Wei 2001; Kozuka *et al.* 2008; Lierke & Holitzner 2008; Andrade, Buiochi & Adamowski 2010). There still exist open questions regarding the limit of

† Email address for correspondence: dpoulikakos@ethz.ch

the acoustic force and the effects of size and viscosity on the exerted force on levitated particles, as well as particle levitation stability.

When a body is exposed to an acoustic field, it experiences a mean force due to the radiation pressure and acoustic streaming. The first analytical treatment of the problem was performed by King (1934) who calculated the force exerted on a small sphere in travelling and standing plane waves. The effect of viscosity on the acoustic force exerted on spheres in an axisymmetric acoustic field with spherical and plane (travelling or standing) waves has been investigated theoretically by Doinikov (1994) and Danilov & Mironov (2000). They defined two limits on radius where the viscosity effects are major or minor.

The dynamics of an acoustically levitated particle has been recently tackled by Barrios & Rechtman (2008). Employing the lattice Boltzmann method and viscous fluid, they observed non-periodic oscillations around the levitation nodes in an axisymmetric levitator. Oscillational instabilities of acoustic levitators were studied by Rudnick & Barmatz (1990), linking the loss of levitation of the sample to the coupling of the particle itself with the acoustic resonance of the chamber, a phenomenon also investigated by Lierke (2002). Droplet stability has received more attention, since an upper limit for acoustic levitation pressure is present, beyond which the sample atomizes (Lee, Anilkumar & Wang 1991). Moreover, frequency-dependent disturbances stimulate the resonant mode of the droplet oscillations, also responsible for the droplet breakup (Yarin *et al.* 2002).

Computational fluid dynamics (CFD) studies of the radiation pressure are uncommon. The first study was reported by Haydock (2005). Recently, a model was developed based on the finite-volume method (FVM) for calculating the acoustic radiation pressure acting on a cylinder (Wang & Dual 2009). They imposed a standing wave as boundary condition, and the fluid–structure interaction and effects of particle shapes were not taken into account. CFD, if adopted properly and validated, provides a powerful tool for the acoustic force estimation and helps provide a better understanding of the physics behind the acoustic levitation. The time-dependency and additional nonlinear phenomena such as effects of viscosity can be studied in more depth with this approach.

In this paper, we investigate the forces exerted on fixed spherical and ellipsoidal particles of a wide range of sizes, in an axisymmetric levitator, for both inviscid and a viscous host fluids, employing validated finite-element method (FEM) and FVM models, respectively. The physical explanations of the effects of fluid viscosity and particle size and shape on the radial and axial forces are provided in detail. The present study sheds light on the issue of particle levitation stability in axisymmetric levitators and provides a comprehensive perspective of the effects of three main parameters influencing particle levitation stability: (*a*) particle axial position; (*b*) particle size, where we find that for large particles, ($R_s/\lambda > 0.25$), the standing wave condition becomes invalid and the radial force exerted on the particle is negative, while for small particles ($R_s/\lambda < 0.01$), the viscous force plays a significant role in inducing instability; and (*c*) particle shape, where we show that for ellipsoidal particles the balance of axial and radial forces is influenced in favour of the radial force affecting stability.

2. Levitation models

The levitator in the present study is an open axisymmetric levitator (Lierke & Holitzner 2008) in a three-node configuration (figure 1*a*). The emitter–reflector height

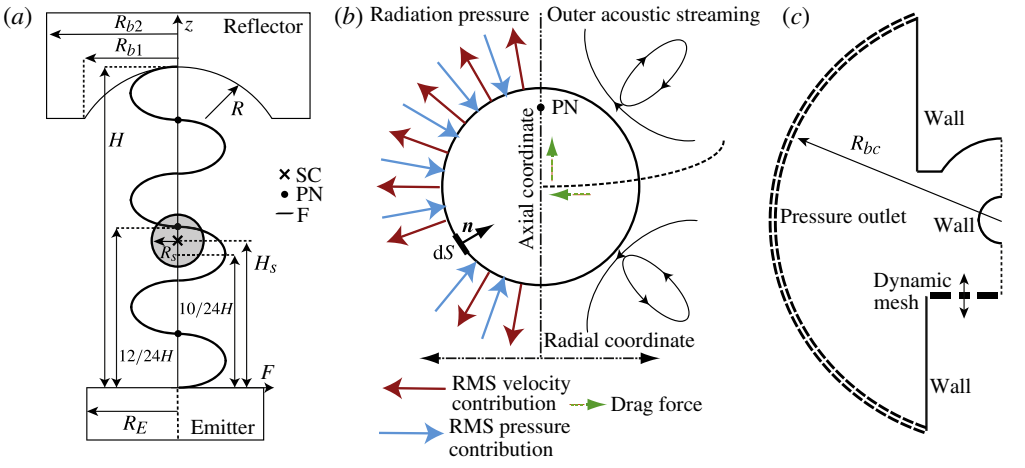

FIGURE 1. (Colour online) (*a*) The levitator and its geometrical parameters. SC, PN and F represent the sphere centre, the pressure node and the axial levitation force along the central axis, respectively. The acoustic force is represented as a sinusoidal function along the vertical axis z and it is positive in the region below the pressure node PN and above the pressure antinode (zero force). The SC is positioned in this area. Here R, R_{b1}, R_{b2} and R_E are the curvature radius, the inner radius and the external radius of the reflector and the radius of the emitter, respectively, H is the distance between emitter and reflector surfaces along the axis and H_s is the distance between the emitter and the centre of the particle along the axis. (*b*) Schematic of r.m.s. velocity and r.m.s. pressure acting on a spherical particle. The acoustic streaming is also shown schematically. (*c*) The computational domain, where R_{bc} is the radius of the outer boundary.

Parameters	Values	Parameters	Values
Frequency (f)	25 kHz	R/λ	2
Temperature (T)	298 K	R_E/λ	0.6
Fluid density (ρ_0)	1.184 kg m^{-3}	R_{b1}/λ	1
Sound speed (c_0)	346 m s^{-1}	R_{b2}/λ	1.1
Wavelength (λ)	13.8 mm	μ (Air)	1.79×10^{-5} Pa
Emitter velocity (V_0)	1 m s^{-1}	μ(Air10)	1.79×10^{-4} Pa
		μ (Air100)	1.79×10^{-3} Pa

TABLE 1. The geometrical and model parameters. The pure inviscid model of Ansys FLUENT exhibited numerical stability problems. Therefore, the simulations for the inviscid case were run with a viscous model with a very small viscosity, five orders of magnitude smaller than that of air and by applying the free slip boundary condition on all of the rigid walls (except for the emitter).

is kept constant. The parameters used are listed in table 1. The cases of inviscid and viscous medium surrounding the levitated particle are modelled sequentially as follows.

2.1. *Inviscid case: FEM model*

An experimentally validated three-dimensional model based on FEM is developed to solve the inviscid medium problem. The inviscid model serves two important

purposes. First, the study of the inviscid case which is computationally much faster than the viscous case and it gives accurate results for small particles in inviscid or low-viscosity medium (Danilov & Mironov 2000). Second, the validation of the subsequent CFD model employed to study the effect of viscosity. The commercial software Simulia Abaqus (6.9-1) based on FEM was used to solve the linear acoustics problem in the frequency domain (see supplementary appendix A, available online at http://dx.doi.org/10.1017/jfm.2012.350). A quarter of the three-dimensional domain was modelled, and on the two orthogonal faces, a zero displacement to the normal component was imposed. Non-reflecting boundary conditions were applied at the outer boundary of the domain and the fluid–structure interaction was modelled between emitter, reflector and acoustic medium. All of the quantities were scaled at the frequency of 1 kHz. The radiation pressure p_r acting on the sphere was calculated using the following equation (King 1934):

$$p_r = \frac{1}{2\rho_0 c_0^2} p_{rms}^2 - \frac{1}{2}\rho_0 v_{rms}^2 \tag{2.1}$$

where p_{rms} and v_{rms} are the root mean square (r.m.s.) pressure and particle velocity in the host fluid, respectively. The total force F_r acting on the particle was obtained by integration of the radiation pressure on the sphere surface S (figure 1*b*):

$$F_r = \int_S p_r \boldsymbol{n}\, \mathrm{d}S. \tag{2.2}$$

A comparison of the numerical and the theoretical results (see supplementary appendix B, available online) is only meaningful for the extreme case where the particle is small ($R_s/\lambda < 0.1$) (Vandaele 2011). No analytical solution is available for the cases where the geometry is complex and/or the particle is large. In order to validate the FEM model, we used the measurements of the axial force acting on a sphere inside an axisymmetric levitator along its central axis reported in (Vandaele 2011; Vandaele, Delchambre & Lambert 2011). The challenge was to adapt the boundary condition of the experiments (pressure measured at the reflector surface) to that of our FEM model. Indeed, the fluid–structure interaction required to impose a displacement on the emitter surface. The results shown in figure 2 prove the ability of our FEM model to accurately estimate the axial force exerted on a sphere.

2.2. *Viscous case: CFD model*

To study the viscosity effect in the range of particle radii of interest, the full axisymmetric Navier–Stokes equations for laminar, compressible flow with ideal gas were solved (figure 1*c*; see also supplementary appendix C, available online) using Ansys FLUENT (ver 12.1). A sinusoidal axial motion at frequency f and velocity V_0 was imposed on the emitter by means of a dynamic mesh (DM). A DM allows accurate estimation of the radiation force on large objects as well as on objects close to the emitter since no standing wave has to be necessarily imposed as a boundary condition. A DM, however, requires the use of a first-order time-discretization scheme and very small time steps for accuracy. Adiabatic condition was assumed at all walls, except at the pressure inlet (at R_{bc}, figure 2*b*), where constant temperature boundary condition was adopted (table 1).

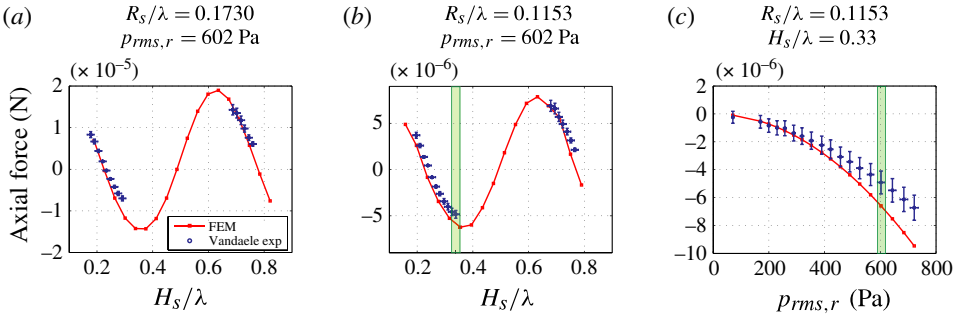

FIGURE 2. (Colour online) Axial force acting on a sphere in the inviscid case at different axial positions. The results are for two radii, $R_s/\lambda = 0.1730$ (*a*) and $R_s/\lambda = 0.1153$ (*b*), at a driving frequency of 40 kHz. A small shift in the axial position z is present, likely due to the different boundary conditions. The FEM simulations were carried out with a constant displacement of the emitter, and the final force was normalized with respect to p_{rms} in correspondence of the reflector and the pressure of the experiment in Vandaele (2011). Experimental points were only given for stable levitation points (see § 3.1). (*c*) The axial force with respect to the levitation power. The p_{rms}^2 scaling law of the levitation force, in accordance with (2.1), is shown. In being conservative, the axial position $H_s/\lambda = 0.33$ represents the worst case of agreement between theory and experiment, as seen in figure 2(*b*).

3. Results and discussion

3.1. *Particle axial position*

The FEM model was used to investigate the axial and radial components of the acoustic force exerted on a sphere of different sizes located at different heights (figure 3). The radial force becomes negative at the height where the axial force is maximum ($H_s/\lambda = 0.73$). This is in accordance with experiments that show that below the altitude of the axial force peak no levitation is possible, because the levitated sample is unstable (Vandaele 2011; Vandaele *et al.* 2011). The radial force behaviour can explain the reason for this instability. When the particle is in the stable region (as for $H_s/\lambda = 0.90, R_s/\lambda < 0.25$ figure 3*b*), the radial force is positive, i.e. the particle is laterally stretched. In this region, the largest contribution to the radiation pressure force is given by the r.m.s. velocity (2.1). The particle is stable because if it moves away from the centre axis, the r.m.s. radial velocity gradient (maximum at the centre axis; see supplementary appendix D, available online) balances the forces and brings the particle back to the centre. When the particle is moved to the right, a lower velocity is present at the right side than at the left side. The corresponding lower pressure on the left side will act as a natural repositioning feedback.

When the particle is in an unstable region (as for $H_s/\lambda = 0.73, R_s/\lambda > 0.25$ figure 3*b*), the radial force is negative, i.e. the particle is laterally compressed. In this region, the largest contribution to the force is given not by the r.m.s. velocity, but by the r.m.s. pressure. The r.m.s. pressure decreases as we move further away from the centre axis. This distribution explains the instability. When the particle moves to the right, a lower pressure is present on the right side than on the left side. Unlike the previous case, this pressure distribution forces the particle to move further away from the centre axis resulting in particle instability and final fall (figure 1*b*).

The maximum particle size that can be stably levitated is around 0.25λ (beyond this value the radial force is negative). However, this value strongly depends on the

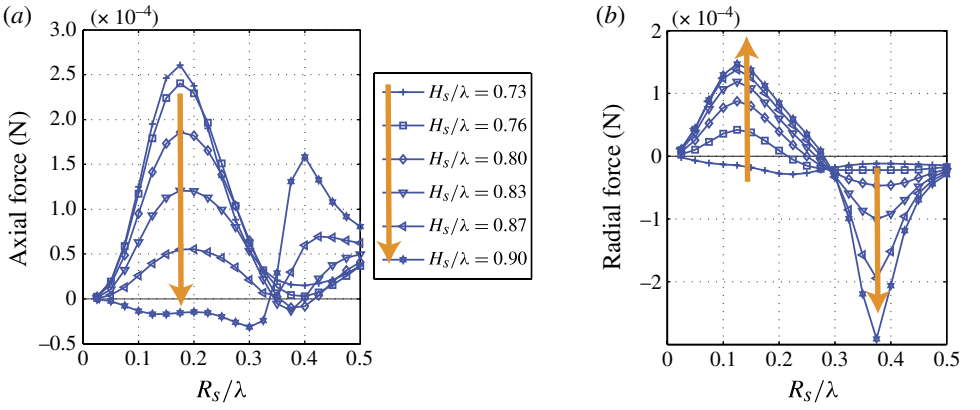

FIGURE 3. (Colour online) The variation of the axial (*a*) and radial (*b*) forces acting on a sphere by varying the radii for different sphere heights H_s/λ.

levitator parameters (R_b, R_a (Lierke & Holitzner 2008) sample shape (Xie & Wei 2004); see § 3.3).

3.2. *Viscous medium-CFD model: sphere*

3.2.1. *Inviscid case limit test*

The axial and radial forces estimated by the CFD and FEM models for $H/\lambda = 1.7$ and $H_s = 11/24H$ (figure 1*a*) are compared in figure 4. The value of H_s is chosen between the pressure node and the axial positive force peak of the central node (figure 1*b*). The normalized sphere radius R_s/λ is varied between 0.025 and 0.5. For small radii ($R_s/\lambda < 0.1$), the axial force increases as a function of R_s^3, as formulated by King (1934) (see supplementary appendix B, available online). For larger radii, the presence of the sphere decreases the acoustic pressure inside the levitator and consequently the force acting on the particle after its peak at $R_s/\lambda = 0.175$. The force becomes even negative at $R_s/\lambda = 0.4$. This phenomenon is due to the reflected waves that are focused on the upper portion of the sphere. By further increasing the particle radius ($R_s/\lambda > 0.4$), the standing wave condition is violated and the axial force rises again due to the establishment of the travelling wave configuration (see supplementary appendix B, available online). Figure 4(*b*) shows the radial force acting on a sphere calculated by the FEM and CFD models. The radial force varies similarly to the axial force with two main differences. It reaches its peak at smaller radius ($R_s/\lambda = 0.125$) and becomes negative for $R_s/\lambda > 0.225$.

The axial forces predicted by the CFD model are in agreement with those by the FEM model for $R_s/\lambda < 0.3$, with the relative difference below 0.05 (figure 4*c*). For $R_s/\lambda > 0.3$, the sharp increase on the relative difference is due to the small absolute value of the axial force (figure 4*a*). A similar behaviour can be observed for the radial force (figure 4*c*). The relative difference shows a peak around the zero-force crossing point ($0.225 < R_s/\lambda < 0.25$). The observed increase in the relative difference for $R_s/\lambda > 0.3$ is likely due to the increase in the oscillation amplitude of the radial force around the asymptotic value for large radii (see supplementary appendix E, available online).

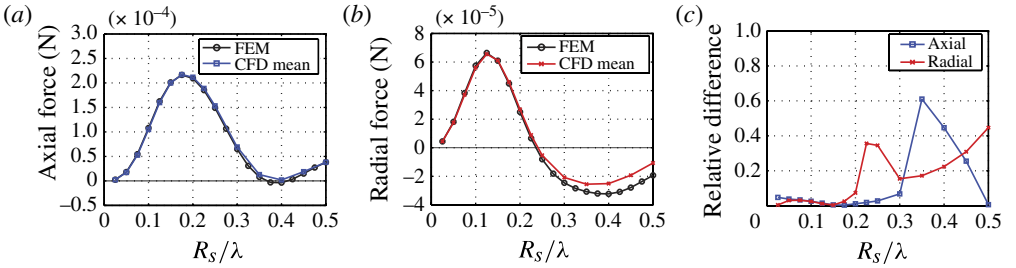

FIGURE 4. (Colour online) (*a*) Axial and (*b*) radial forces acting on a sphere by varying its radius at $H_s/\lambda = 0.78$. FEM represents the force calculated from (2.1) using the r.m.s. pressure and velocity obtained by the FEM model. CFD mean represents the mean force acting on the sphere averaged over the last 50 periods of 150 periods; (*c*) relative differences between the forces calculated by the two models.

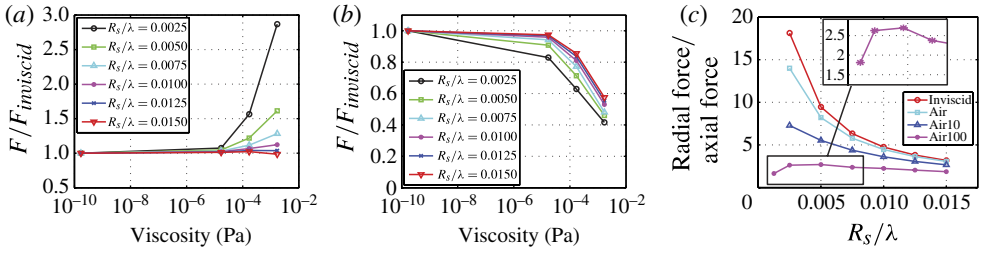

FIGURE 5. (Colour online) The normalized (*a*) axial and (*b*) radial forces versus viscosity for small radii ($R_s/\lambda \leqslant 0.0150$). The normalization is relative to the inviscid case; (*c*) the ratio of radial to axial forces acting on a small spherical particle for different medium viscosity.

3.2.2. *Effect of viscosity*

Utilizing the validated CFD model, the effect of medium viscosity on the force exerted on the levitated object is investigated. This effect is important as it may induce instability of the levitated particle (Danilov & Mironov 2000). It has been shown that only when the dimension of the object becomes comparable to the acoustic boundary layer thickness $\delta_u = \sqrt{\mu/(\rho\pi f)}$ (see supplementary appendix F, available online), the viscous effects play a role (Doinikov 1994; Danilov & Mironov 2000; Haydock 2005; Wang & Dual 2009). Since the viscosity of air is relatively low, δ_u is very small (at $f = 25$ kHz, $\delta_u = 14\ \mu\text{m} = 0.001\lambda$). In microfluidics, the viscous effect is a typical issue for acoustofluidics (Bruus *et al.* 2011). For large droplets, this effect can be important for levitation in an immiscible host fluid (Busse 1984; Annamalai, Trinh & Wang 1985; Trinh *et al.* 1998), with δ_u entering the millimetre range. This work focuses on rigid spheres in a viscous medium for the parameters given in table 1, the results however can be extended to other cases by normalizing the values. Referring to (Haydock 2005) and considering λ to be the characteristic length of the domain, we have a non-dimensional dynamic viscosity of $\nu = 0.00182$ for air at 25 kHz.

In figure 5(*a*,*b*), the axial and radial forces exerted on a sphere in a viscous fluid normalized with respect to those in an inviscid fluid for small radii ($0.0025 < R_s/\lambda < 0.0150$) are shown. For small particles, the axial force increases with an increase in viscosity (figure 5*a*), which is in agreement with (Doinikov 1997; Wang & Dual 2009).

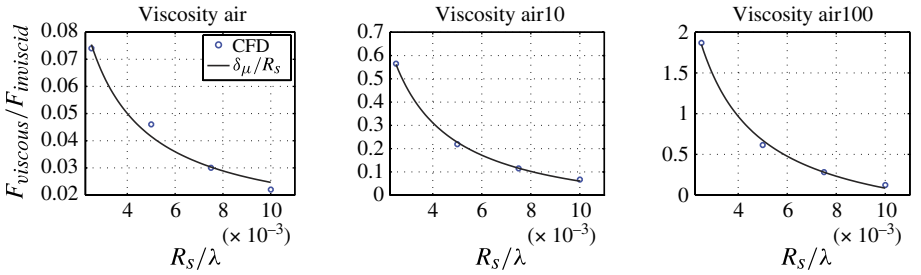

FIGURE 6. (Colour online) The $1/R_s$ fit is very good for high viscosity (coefficient of determination ranged from 0.997 to 0.999), while for small viscosity, the very small difference from the inviscid case (0.02–0.07) may be responsible for a slightly less accurate fit (coefficient of determination is equal to 0.982). The maximum δ_u/R_s is 4 for Air100. In spite being beyond the limit of weak dissipative effects, ($\delta_u/R_s \ll 1$), the relationship in (3.1) is still valid.

For R_s/λ slightly larger than 0.0125, the axial force starts to decrease with increasing viscosity. This behaviour is not the same for the radial force (figure 5*b*) which always decreases with increasing viscosity. Doinikov (1997) provided an analytical solution for the axial force acting on a sphere in a viscous fluid (equation (30) in Doinikov (1997)). Considering all of the assumptions of the solution (plane standing wave, $R_s \ll \lambda$, $\rho_{sphere} \gg \rho$, and negligible thermal effects), it can be shown that for weak dissipative effects the viscous contribution scales with δ_u/R_s (figure 6):

$$F = F_{inviscid} + F_{viscous}, \quad F_{viscous} \propto F_{inviscid}\frac{\delta_u}{R_s}. \tag{3.1}$$

The additional parameter affecting the total mean force exerted on small particles is the drag force due to the acoustic streaming (see supplementary appendix G, available online). For the radial force, the drag force acts laterally compressing the sphere, hence, against the 'restoring' radial force as can be inferred from figure 1(*b*). Therefore, as the viscosity increases, the increased streaming further reduces the radial force. For the axial force, the streaming patterns are not symmetric about the horizontal axis of the particle. For rigid bodies, the drag force of the streaming acts in favour of the radiation force and increases the total force (Lee & Wang 1990). For droplets in a highly viscous fluid, the internal liquid flow will be coupling with the external acoustic streaming (Rednikov *et al.* 2006). However, the vorticity inversion is responsible for the possible change of direction of the axial force, not for the radial force. The drag force on the radial component is always negative. The above discussion explains the different behaviour of the axial and radial forces due to a change in viscosity for small radii.

For small particles in viscous fluid, an increase in viscosity reduces the radial force to the axial force ratio, affecting stability (figure 5*c*). In the range of small radii studied, the ratio of radial to axial forces increases with decreasing the sphere size, except for high viscosities and very small radii where this dependence is not monotonic (see the zoom in figure 5*c*). This hints toward approaching force inversion and instability of very small particles in acoustic levitation (i.e. aerosols). Indeed, for large δ_u/R_s (not in the range of this study) the viscous forces act in the direction opposite to the pressure node (Danilov & Mironov 2000).

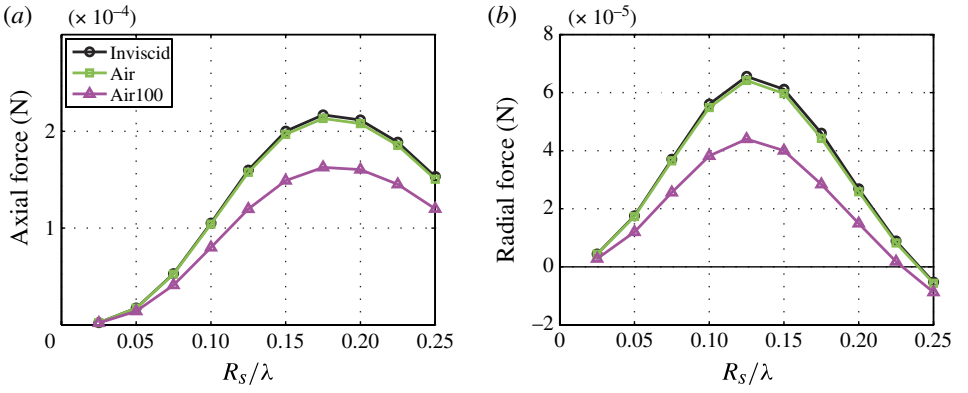

FIGURE 7. (Colour online) The axial (*a*) and radial (*b*) forces acting on a sphere as function of R_s/λ.

	Pressure r.m.s. (Pa)	Velocity r.m.s. (m s^{-1})
Inviscid	2661	5.53
Air	2650 (99.5 % of inviscid)	5.2 (94.0 % of inviscid)
Air100	2311 (86.8 % of inviscid)	4.5 (81.4 % of inviscid)

TABLE 2. Maximum r.m.s. pressure and velocity into the levitator with very small particles ($R_s/\lambda = 0.0025$, i.e. no interference to the acoustic field) by varying viscosity.

Figure 7 shows how the axial and radial forces decrease with increasing viscosity for large spheres ($0.025 < R_s/\lambda < 0.25$) for three different viscosities (inviscid, Air and Air100). As was already stated, for large spheres ($R_s/\lambda \geqslant 0.0125$), the axial and radial forces always decrease with increasing viscosity. When the viscosity increases, the r.m.s. pressure and velocity inside the chamber decrease (the movement of the radiating plate is the imposed boundary condition). Consequently, the mean force due to the acoustic pressure decreases (2.1). The value of δ_μ/R_s and the relative drag force are too small to appreciably contribute in this case. As shown in figure 7(*b*), the trend of variation of the radial force with viscosity continues in the negative force region. As was already mentioned, when the radial force is negative, the r.m.s. pressure contribution to the radiation pressure takes over the r.m.s. velocity contribution. When the viscosity increases, the decrease in the r.m.s. pressure is less than that in the r.m.s. velocity (table 2). Therefore, the magnitude of the radial force increases with increasing viscosity (see supplementary appendix H, available online).

3.3. *Viscous medium-CFD model: ellipsoid*

In an axisymmetric levitator, it is of interest to study ellipsoidal objects. Indeed, during the levitation of droplets this represents a typical shape (Yarin *et al.* 1998). As seen in figure 4, the axial force induces a compression of the droplet along its semiminor axis *a*, while the radial force stretches the droplet along its semimajor axis *b*. To compare the result to the spherical case, we introduce an equivalent radius which preserves

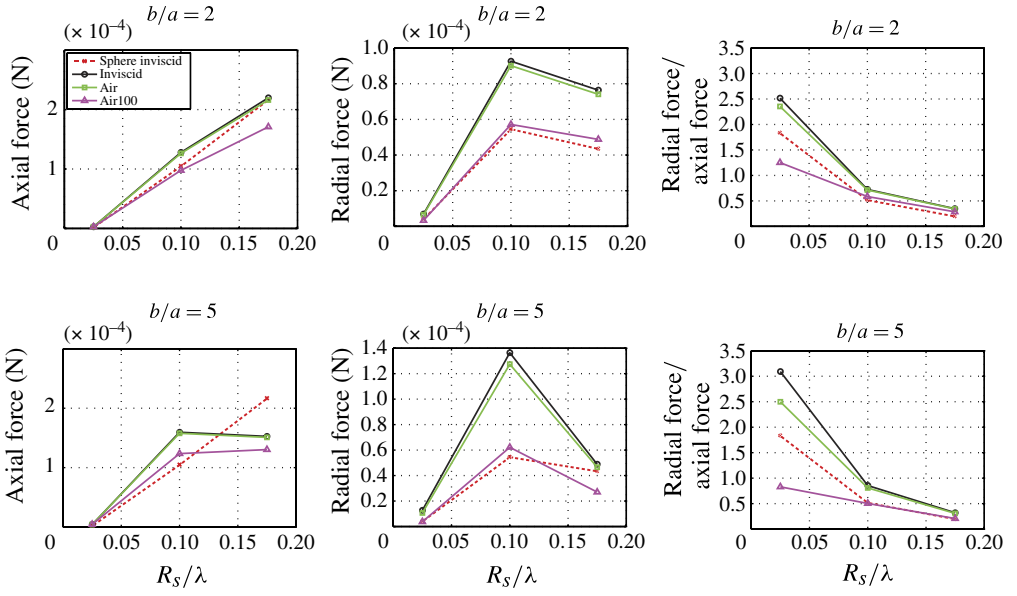

FIGURE 8. (Colour online) Axial and radial forces acting on an ellipsoid of $b/a = 2$ and 5.

volume (see supplementary appendix I, available online):

$$V_{sphere} = V_{ellipsoid}, \quad R_{eq} = R_s = \sqrt[3]{b^2 a}. \tag{3.2}$$

Figure 8 shows the axial and radial forces acting on ellipsoids with different radii ($b/a = 2$ and 5). The magnitude of the radial force becomes more than two times that of the axial force for $b/a = 5$ in the case of small radii. On the other hand, high positive radial force means high stability in the axial position. Different from a sphere and an ellipsoid with a modest aspect radio ($b/a = 2$), for $b/a = 5$, the axial force is lower for a larger ellipsoid ($R_s/\lambda = 0.175$) than that for a smaller one ($R_s/\lambda = 0.1$), which is due to the actual dimension of the ellipsoid ($b/\lambda = 0.299$). At this size, the object acts as an obstacle to the establishment of the standing wave in the levitator, resulting in a lower acoustic pressure. Also, the radial force for both $b/a = 2$ and 5 is higher for an ellipsoid than that for the volume-equivalent sphere. The reason is due to the higher velocity at the horizontal axis extremities of the ellipsoid compared with the sphere. The higher velocity results in higher stretching, i.e. larger radial force. Another observation is that an increase in viscosity reduces the radial force more significantly than the axial force. This could be due to strongly reduced velocity at the horizontal axis extremities of the ellipsoid with increasing viscosity (see supplementary appendix I, available online). Figure 8 shows that for ellipsoidal particles the balance of axial and radial forces is influenced in favour of the radial force improving the particle levitation stability.

4. Conclusion

The issue of stability of a particle in an acoustic levitator was investigated, focusing on the effects of particle size and medium viscosity on the axial and radial forces exerted on fixed spherical and ellipsoidal particles. The radial force always decreases with increasing viscosity, while the axial force behaviour is non-monotonic, depending

on the radius of the particle. The cross-over value of the radius for our configuration was around 1 % of the wavelength λ. The physical explanation for the effect of viscosity on the force acting on both small and large particles was discussed in detail. The force exerted on an ellipsoidal particle was found to be stronger than that exerted on a volume-equivalent sphere up to the point where its size becomes large enough to act against the establishment of the standing wave in the levitator chamber. Based on the findings in this paper, insight for the phenomenon of particle levitation instability in an acoustic levitator was provided. It was found that the radial force behaviour can explain levitation instability. At intrinsically unstable axial positions, the radial force is negative. For large particles, particle stability is lost due to the radial force becoming negative and for small particles the viscous force can induce instability. A levitated ellipsoidal particle is more stable than its volume-equivalent spherical particle.

Acknowledgements

Funding from the Swiss National Science Foundation (SNSF), grant no. 200021-122169 and the contribution of Gianluca Engeler, ETH Zurich are gratefully acknowledged.

Supplementary data

Supplementary data are available at http://dx.doi.org/10.1017/jfm.2012.350.

REFERENCES

ANDRADE, M. A. B., BUIOCHI, F. & ADAMOWSKI, J. C. 2010 Finite element analysis and optimization of a single-axis acoustic levitator. *IEEE Trans. Ultrason. Ferroelectr.* **57**, 469–479.

ANNAMALAI, P., TRINH, E. & WANG, T. G. 1985 Experimental study of the oscillations of a rotating drop. *J. Fluid Mech.* **158**, 317–327.

BARMATZ, M. & COLLAS, P. 1985 Acoustic radiation potential on a sphere in plane, cylindrical, and spherical standing wave fields. *J. Acoust. Soc. Am.* **77**, 928–945.

BARRIOS, G. & RECHTMAN, R. 2008 Dynamics of an acoustically levitated particle using the lattice Boltzmann method. *J. Fluid Mech.* **596**, 191–200.

BJELOBRK, N., FORESTI, D., DORRESTIJN, M., NABAVI, M. & POULIKAKOS, D. 2010 Contactless transport of acoustically levitated particles. *Appl. Phys. Lett.* **97**, 161904.

BRUUS, H., DUAL, J., HAWKES, J., HILL, M., LAURELL, T., NILSSON, J., RADEL, S., SADHAL,S. & WIKLUND, M. 2011 Forthcoming lab on a chip tutorial series on acoustofluidics: Acoustofluidics-exploiting ultrasonic standing wave forces and acoustic streaming in microfluidic systems for cell and particle manipulation lab chip. *Lab on a Chip* **11**, 3579–3580.

BUSSE, F. H. 1984 Oscillations of a rotating liquid-drop. *J. Fluid Mech.* **142**, 1–8.

DANILOV, S. D. & MIRONOV, M. A. 2000 Mean force on a small sphere in a sound field in a viscous fluid. *J. Acoust. Soc. Am.* **107**, 143–153.

DOINIKOV, A. A. 1994 Acoustic radiation pressure on a compressible sphere in a viscous fluid. *J. Fluid Mech.* **267**, 1–21.

DOINIKOV, A. A. 1997 Acoustic radiation force on a spherical particle in a viscous heat-conducting fluid. Part 2. Force on a rigid sphere. *J. Acoust. Soc. Am.* **101**, 722–730.

FORESTI, D., BJELOBRK, N., NABAVI, M. & POULIKAKOS, D. 2011 Investigation of a line-focused acoustic levitation for contactless transport of particles. *J. Appl. Phys.* **109**, 093503.

FORESTI, D., NABAVI, M. & POULIKAKOS, D. 2012 Contactless transport of matter in the first five resonance modes of a line-focused acoustic manipulator. *J. Acoust. Soc. Am.* **131**, 1029–1038.

HAYDOCK, D. 2005 Lattice boltzmann simulations of the time-averaged forces on a cylinder in a sound field. *J. Phys. A: Math Gen.* **38**, 3265–3277.

KING, L. V. 1934 On the acoustic radiation pressure on spheres. *Proc. R. Soc. Lond.* A. **147**, 212–240.

KOYAMA, D. & NAKAMURA, K. 2010 Noncontact ultrasonic transportation of small objects over long distances in air using a bending vibrator and a reflector. *IEEE Trans. Ultrason. Ferroelectr.* **57**, 1152–1159.

KOZUKA, T., YASUI, K., TUZIUTI, T., TOWATA, A. & IIDA, Y. 2008 Acoustic standing-wave field for manipulation in air. *Japan J. Appl. Phys.* **47**, 4336–4338.

LEE, C. P., ANILKUMAR, A. V. & WANG, T. G. 1991 Static shape of an acoustically levitated drop with wave-drop interaction. *Phys. Fluids* A **3**, 2497–2515.

LEE, C. P. & WANG, T. G. 1990 Outer acoustic streaming. *J. Acoust. Soc. Am.* **88**, 2367–2375.

LIERKE, E. G. 2002 Deformation and displacement of liquid drops in an optimized acoustic standing wave levitator. *Acta Acust. United Ac.* **88**, 206–217.

LIERKE, E. G. & HOLITZNER, L. 2008 Perspectives of an acoustic-electrostatic/electrodynamic hybrid levitator for small fluid and solid samples. *Meas. Sci. Technol.* **19**, 115803.

REDNIKOV, A. Y., ZHAO, H., SADHAL, S. S. & TRINH, E. H. 2006 Steady streaming around a spherical drop displaced from the velocity antinode in an acoustic levitation field. *Q. J. Mech. Appl. Maths* **59**, 377–397.

RUDNICK, J. & BARMATZ, M. 1990 Oscillational instabilities in single-mode acoustic levitators. *J. Acoust. Soc. Am.* **87**, 81–92.

TRINH, E. H., THIESSEN, D. B. & HOLT, R. G. 1998 Driven and freely decaying nonlinear shape oscillations of drops and bubbles immersed in a liquid: experimental results. *J. Fluid Mech.* **364**, 253–272.

VANDAELE, V. 2011 Contactless handling for micro-assembly: acoustic levitation, PhD thesis.

VANDAELE, V., DELCHAMBRE, A. & LAMBERT, P. 2011 Acoustic wave levitation: handling of components. *J. Appl. Phys.* **109**, 124901.

WANG, J. T. & DUAL, J. 2009 Numerical simulations for the time-averaged acoustic forces acting on rigid cylinders in ideal and viscous fluids. *J. Phys. A – Math. Theor.* **42**.

XIE, W. J. & WEI, B. 2001 Parametric study of single-axis acoustic levitation. *Appl. Phys. Lett.* **79**, 881–883.

XIE, W. J. & WEI, B. 2004 Dynamics of acoustically levitated disk samples. *Phys. Rev.* E **70**, 046611.

YARIN, A. L., PFAFFENLEHNER, M. & TROPEA, C. 1998 On the acoustic levitation of droplet. *J. Fluid Mech.* **356**, 65–91.

YARIN, A. L., WEISS, D. A., BRENN, G. & RENSINK, D. 2002 Acoustically levitated drops: drop oscillation and break-up driven by ultrasound modulation. *Intl J. Multiphase Flow* **28**, 887–910.